SUPPORTING MATERIAL

Mechanical checkpoint for persistent cell polarization in adhesion-naive fibroblasts

Philippe Bun,[†§] Jun-Jun Liu,[†] Hervé Turlier,[‡,§] ZengZhen Liu,[†]
Jean-François Joanny[‡] and Maïté Coppey-Moisan[†*]

[†]Macromolecular Complexes in Living Cells (CNRS-UMR7592),
Institut Jacques Monod,
Universit Paris VII, 75205 Paris, France,

[‡]Physicochimie Curie (CNRS-UMR168),
Institut Curie, Section de Recherche,
26 rue d'Ulm, 75248 Paris Cedex 05, France,

[§]Present adress: European Molecular Biology Laboratory,
Meyerhofstrasse 1, D-69117 Heidelberg, Germany

[*]Corresponding Author: coppey.maite@ijm.univ-paris-diderot.fr

Supporting figures

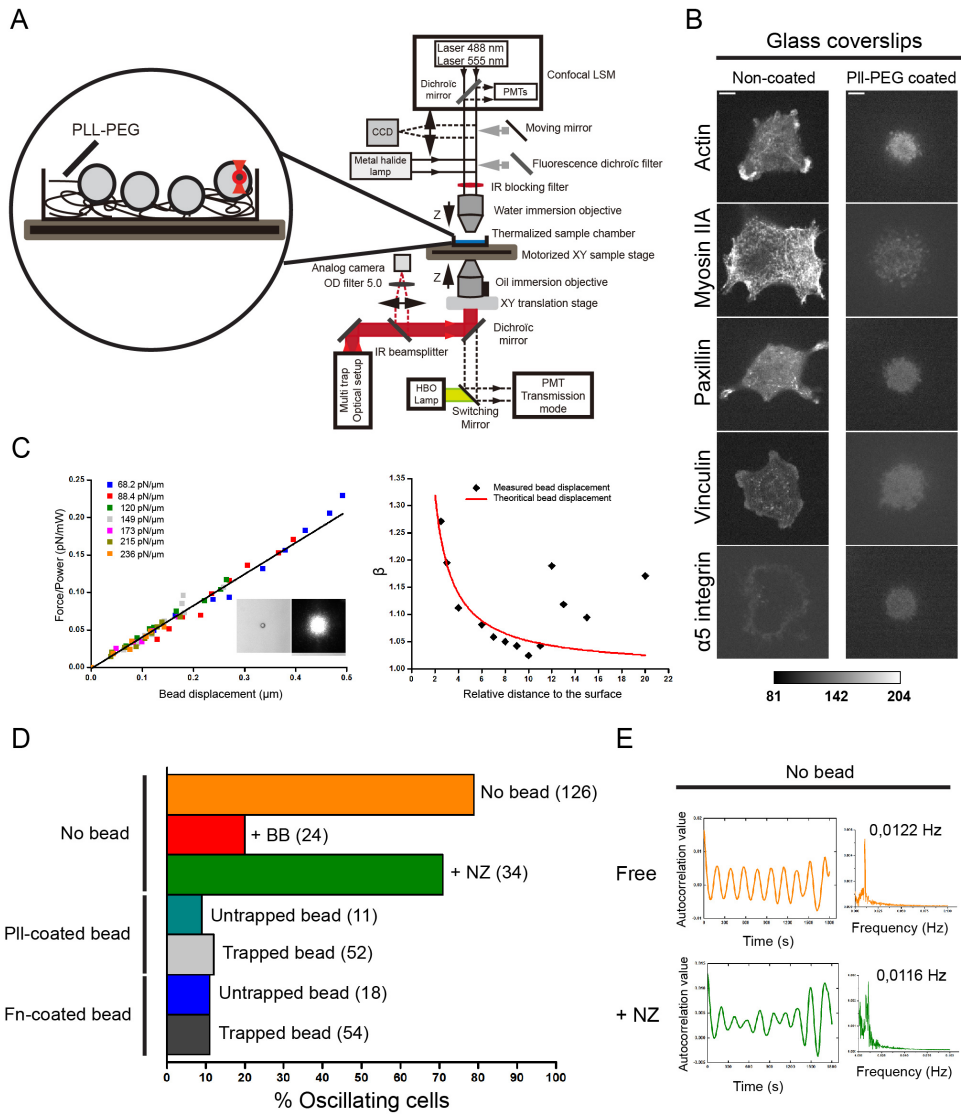

Fig. S1. Experimental approach for monitoring cell oscillation and polarization. **(A)** Schematic representation of the dual objective system. The multiple optical trap system is adapted onto an upright microscope. The epi-fluorescence imaging configuration can be either in confocal or widefield mode by adding a fluorescence dichroïc filter and mirror. Transmitted light imaging can be obtained either in confocal mode on the PMT positioned

at the back of the trapping objective or in widefield mode from the HBO lamp to CCD camera by switching a mirror. An analog camera was added to visualize the optical trap by imaging IR laser reflection. Inset, schematics depicting the experimental condition. 3T3 fibroblast cell is suspended in a microscopy chamber mounted with a Pll-PEG-coated glass coverslip. A single coated bead is then trapped and positioned on the cell cortex. During the whole experiment, cells did not move into the optical trap. **(B)** Suspended cells were prevented from adhesion. To verify this, fluorescent images were acquired at the same imaging plane, close to the glass cover slips bottom. No specific protein organization or clusters were observed for treated cover slips two hours after cell suspension whereas adhesion sites and ruffling membranes were detected in the absence of cover slip treatment. Scale bars, 5 μm. **(C)** Right: Force/Power-displacement curve for a single trapped bead. The black line corresponds to the linear fit forced through zero corresponding to 401 $pN.\mu m^{-1}.W^{-1}$. (Insets) Transmission image of a 1.7 μm-diameter polystyrene latex bead and the corresponding optical trap imaged onto the CCD camera. Left: corrected drag coefficient, β. One bead is trapped and its displacement within the trap measured at fixed oscillation and fixed laser power to 241 mW at different relative distances from the surface. The red curve corresponds to the theoretical curve (given by Faxens law). The increase in bead displacement from the expected value at 12 μm and at 20 μm from the surface corresponds to trap stiffness degradation of 3% and 11%, respectively. At 8 μm above the surface, the relative difference in stiffness was 1.4%. This result corresponds to the relative error on the measured trap stiffness. Here, we choose to trap up to 11 μm above the glass cover slips. **(D)** Histograms showing the percentage of oscillating cells depending on the mechanical and adhesive conditions of the experiment. Total numbers of analyzed cells are indicated. **(E)** Frequency of cell oscillation. Fast Fourier transforms are performed on temporal autocorrelation curves extracted from cortical actomyosin kymographs in the absence (Fig. 3 A and Fig. S2 A) or in the presence of NZ (Fig. 4 A,B). We extract a main peak frequency corresponding to the cell oscillation frequency. These values are indicated on curves.

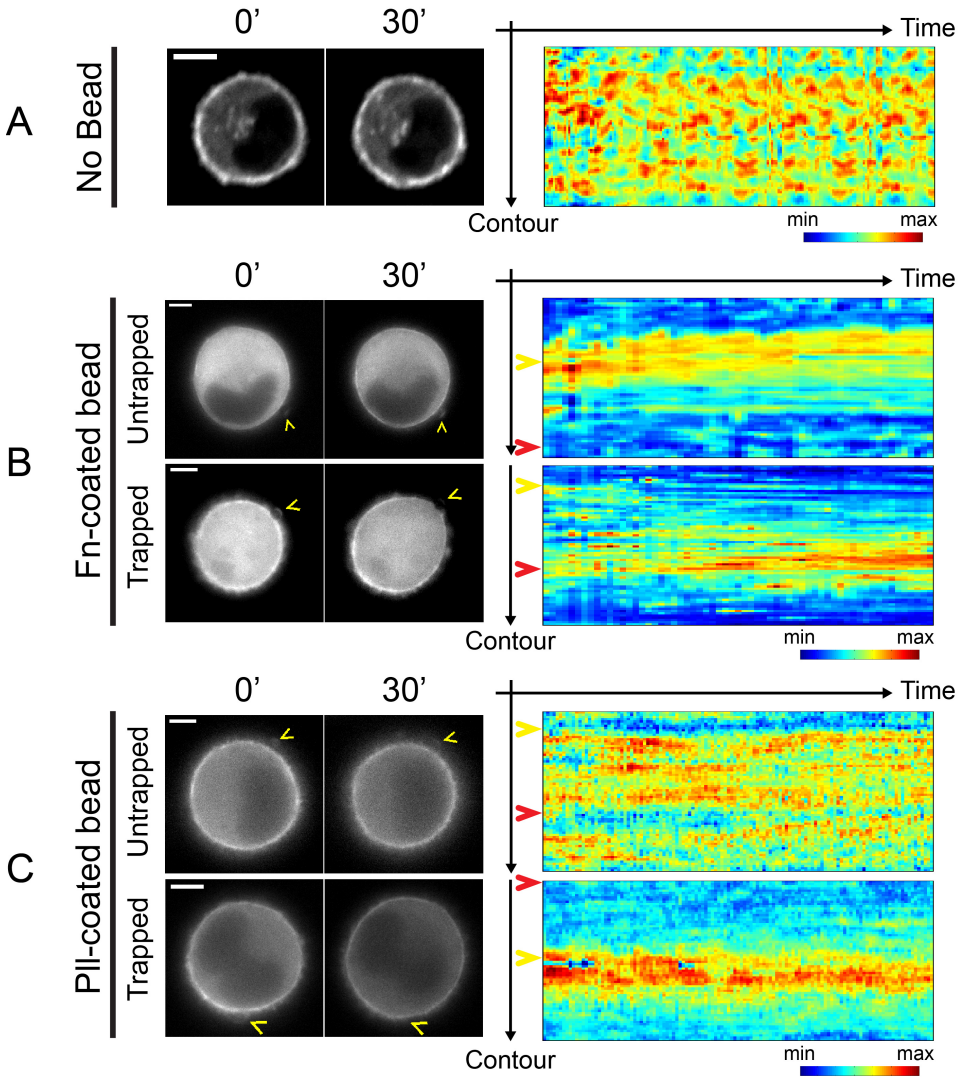

Fig. S2. Cell shape polarization is sustained by a polarized cortical actin distribution. **(A-C)** Monitoring of the cortical dynamics of actin. Similar effects are observed for cortical myosin IIA. Left: Fluorescence images of a single non-adherent 3T3 cell expressing eGFP-actin acquired in different mechanical and adhesive conditions: in the absence of any stiff and adhesive cue **(A)**, in the presence of a single Fn-coated bead **(B)** and Pll-coated bead **(C)**. Yellow arrowheads indicate the position of the inductive trigger. Right: Cell contour kymographs show the evolution of fluorescence intensity of cortical actin over time. Yellow arrowheads indicate the cortical angular position of the trigger whereas red arrowheads point out the opposite pole. Representative contour kymographs is displayed for each condition. All scale bars, 5 μm.

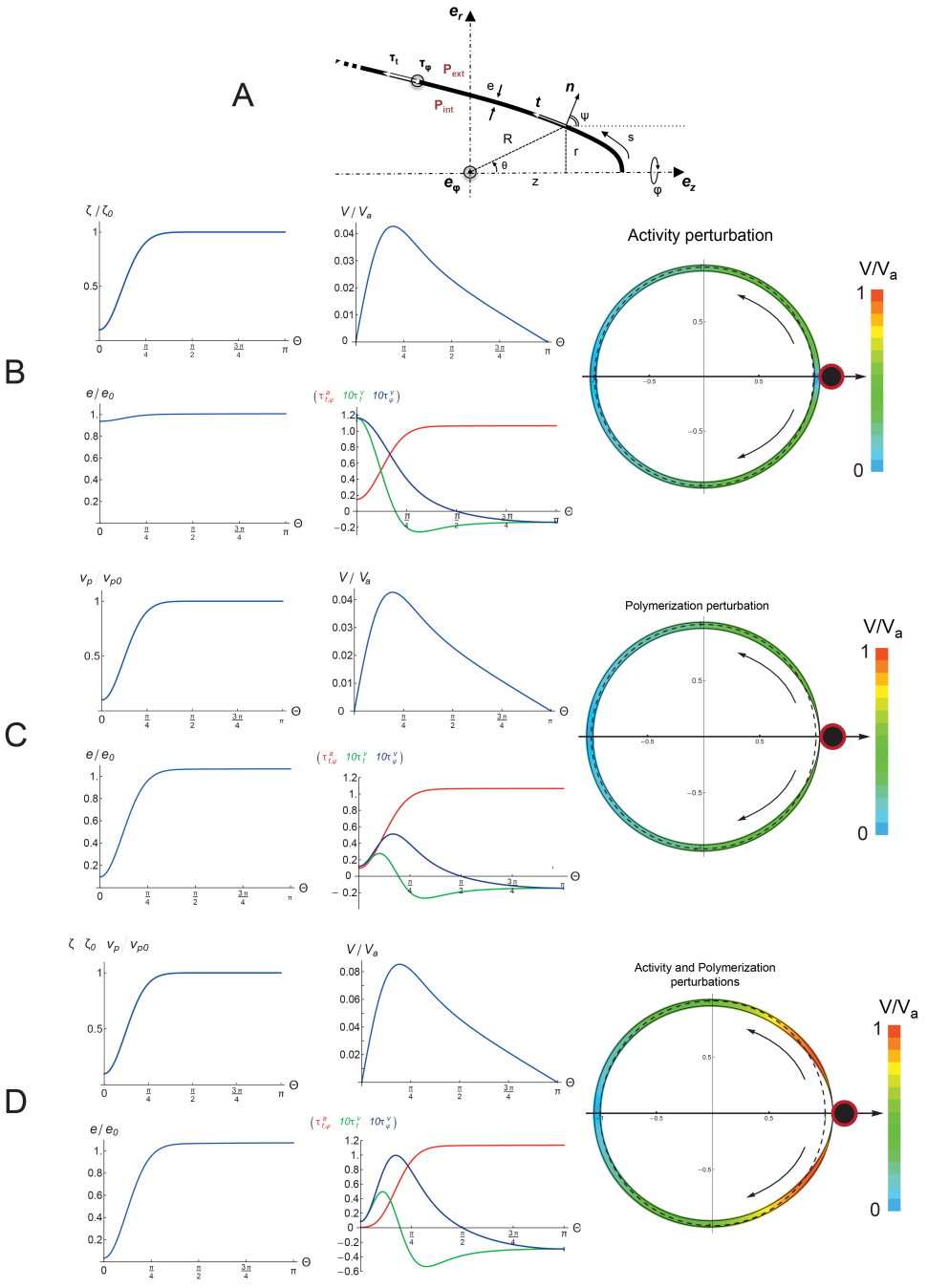

Fig. S3. Active membrane shell model of the cell cortex. **(A)** Schematic of a merid-

ional section of the axisymmetric membrane shell of thickness e, described in the local Eulerian Frenet frame $(\boldsymbol{t}, \boldsymbol{n}, \boldsymbol{e_\varphi})$ by either spatial (z, r), polar (θ, r) or curvilinear (s, ψ) coordinates. The membrane shell is under tension: τ_t and τ_φ respectively in its tangential and azimuthal directions $(\boldsymbol{t}, \boldsymbol{e_\varphi})$, and is submitted to the pressure difference $P_{\text{int}} - P_{\text{ext}}$ along its normal direction $\boldsymbol{n}$ (*Right*). **(B-D)** Results of the model for a local perturbation in the bead region of myosin activity **(B)**, polymerization **(C)** or both simultaneously **(D)**: (ζ/ζ_0, v_p/v_{p0}) Form of the activity $\zeta(\theta)$ or polymerization $v_p(\theta)$ perturbation function imposed along the cortex as a function of the angle θ. (V/V_a) Amplitude of the cortical flow $V(\theta)$ generated by the perturbation, normalized by a typical active velocity $V_a = R_0 \frac{\zeta_0 \Delta\mu}{\eta}$, along the cortex as a function of θ. (e/e_0) Distribution of the cortical thickness $e(\theta)$ along the cortex, normalized by the initial thickness e_0. ($\tau^a_{t,\varphi}$ $10\tau^v_t$ $10\tau^v_\varphi$) Cortical tension as function of θ: isotropic active tension $\tau^a_{t,\varphi}(\theta)$ (*red*) and anisotropic viscous tensions $\tau^v_t(\theta) \neq \tau^v_\varphi(\theta)$ (*green, blue*), multiplied by a prefactor 10; they lead to the stationary non-spherical shape of the cell at mechanical equilibrium. (*Right*) Cell shape, cortical thickness and cortical flow amplitude after perturbation; the arrows indicate the direction of the cortical flow. (Fig. S3D *Right* corresponds to Fig. 5 *Right* in the main text).

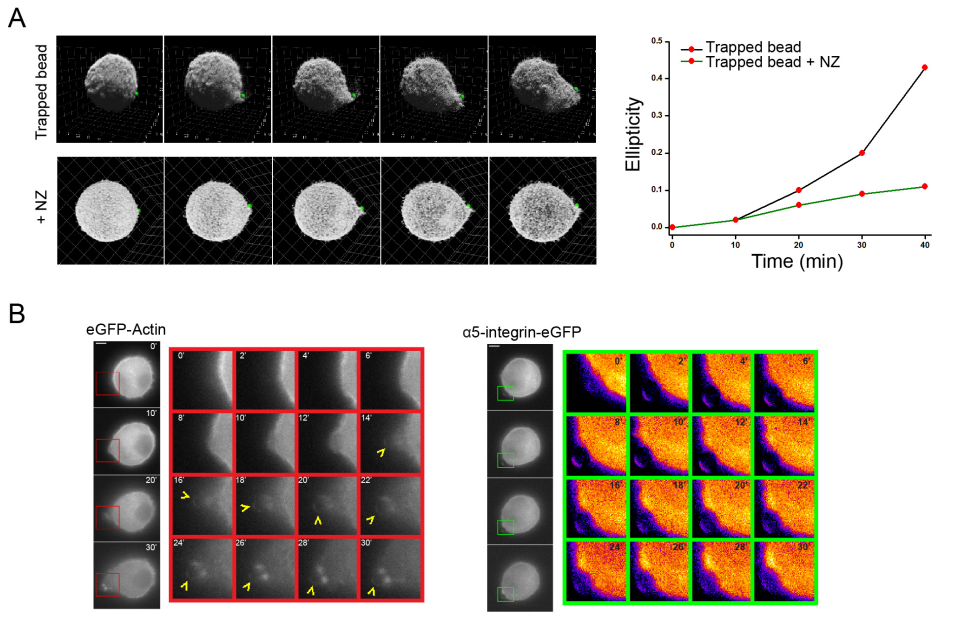

Fig. S4. Establishment of an intracellular polarity, concomitant with the MT-dependent growth of a 3D protrusion. **(A)** 3D reconstructions of non-adherent 3T3 cells subjected to a single trapped Fn-coated bead in the absence (top) and in the presence (bottom) of NZ. Green dots indicate the bead position. Right: Cell shapes are fitted with an ellipsoid, and ellipticity are calculated and displayed every 10 min. **(B)** Left: Time-lapse fluorescence imaging of a 3T3 cell expressing eGFP-actin. Montage of cropped fluorescent images at the bead-containing plane, corresponding to the region of the cell in the red box is shown. Recruitment of actin proteins is only visible 12 to 18 min after the application of a single Fn-coated bead. Addition of drugs (NZ or BB) as well as the attachment of Fn-coated beads does not lead to actin protein recruitment. The yellow arrowheads point at the position of the coated bead. Right: 3T3 cells expressing α5-integrineGFP were observed for 30 min. Montage of cropped fluorescent images corresponding to the region of the cell in the green box is shown. We observed an accumulation of α5-integrin proteins which is temporally correlated with actin proteins recruitment upon the application of a single Fn-coated bead. Images were acquired every 2 min for 30 min. All scale bars, 5 μm.

Supporting model

Local perturbation of an active viscous membrane shell theory

We develop a physical model for describing the dynamics of the cell cortex based on the active-gel theory (1). We explicit mechanical force balance and mass conservation for the cortical layer, which is under permanent turnover and subject to intra-and extracellular pressures. We reduce the equations to a mechanical membrane shell theory by remarking that the cortex layer is very thin compared to the cell curvature radii. We finally consider that the mechanical equilibrium within the cytosol is very rapid compared to the slow deformation of the cortex (about $20min$). We therefore consider the internal cell pressure P_{int} as uniform. This is justified experimentaly by the absence of visible cytosolic flow within the cell on our observation time-scales. The Eulerian model of the cortex formulated in this paper is equivalent to the Lagrangian active viscous membrane shell theory proposed in (2) for describing cell cortex deformation during cytokinesis.

The model predicts the cell shape and the actomyosin distribution along the cell surface, given the myosin motor activity and polymerization within the cortex. These parameters are indeed actively and locally tightly regulated by the cell, and are used as prescribed inputs in the model. However we use an approximate method to solve the mechanical equations that only considers small perturbations of the different variables from a given reference state chosen as a spherical cell. The results remain limited to small amplitudes, since the system is weakly perturbed, but they reveal the fundamental physical principles at work. Solving the coupled non-linear equations beyond perturbation theory is a complex numerical problem (2) which is beyond the scope of this work. We therefore do not intend to make quantitatively accurate results, but rather to bring out and rationalize the essential mecanisms involved in the cortical redistribution and cell shape change upon the adhesion-cue trigger. We propose nonetheless a physically fully consistent scenario for the cell polarization by a local biomechanical trigger, and in very good qualitative agreement with experimental observations.

Theoretical description of the model

Mechanical equilibrium of an axisymmetric membrane shell

We write the mechanical equilibrium for a membrane shell, that is to say a thin shell where the contribution of stress moments and shearing forces are neglected compared to the tensions (3). The local ratio of shell torques and shell tensions can indeed be evaluated as of the order of $\left(\frac{e}{R}\right)^2$ where e is the local thickness of the shell and R is the local mean curvature radius. A membrane shell theory can be therefore expressed in terms of tensions only and remains valid as far as the shell remains thin relative to local curvature radii, which is clearly the case of our cells during polarization (Fig. 3 B; Fig. S2 B and Movie S3).

Polarized cells remain furthermore symmetric around an axis crossing the center of the cue region in experiments (3D reconstruction, Fig. S3 A). We write therefore the mechanical equilibrium for an axisymmetric membrane shell in the Eulerian local Frenet frame $(\boldsymbol{t}, \boldsymbol{n}, \boldsymbol{e_\varphi})$ as defined in Fig. 5 and Fig. S3 A.

The first equation of equilibrium is the balance of forces normal to the membrane shell and relates the pressure difference accross the cell $\Delta P \equiv P_{\text{int}} - P_{\text{ext}}$ to local membrane

shell tensions multiplied by curvatures (1).

$$\Delta P = \tau_t \, \kappa_t + \tau_\varphi \, \kappa_\varphi. \tag{1}$$

τ_t, τ_φ are the tensions acting in the principal directions: respectively in the tangential and azimuthal directions, $\boldsymbol{t}$ and $\boldsymbol{e_\varphi}$. The corresponding principal curvatures are defined in terms of the intrinsic curvilinear coordinates (s, ψ) by

$$\kappa_t = \frac{\partial \psi}{\partial s}, \tag{2a}$$

$$\kappa_\varphi = \frac{\sin \psi}{r}. \tag{2b}$$

The curvilinear coordinates are related to spatial coordinates by the following differential relations

$$dr = \cos \psi \, ds, \tag{3a}$$

$$dz = \sin \psi \, ds. \tag{3b}$$

The second equilibrium equation is the balance of forces tangentially to the meridional contour (4)

$$\frac{\partial \tau_t}{\partial s} + \frac{\tau_t - \tau_\varphi}{r} \frac{dr}{ds} = 0. \tag{4}$$

which can be written equivalently

$$\frac{\partial r \tau_t}{\partial r} = \tau_\varphi. \tag{5}$$

Membrane shell tensions

At first order in e/R, the two principal tensions of the membrane shell are simply given by

$$\tau_t = e \, \sigma_{tt}, \tag{6a}$$

$$\tau_\varphi = e \, \sigma_{\varphi\varphi}. \tag{6b}$$

where $(\sigma_{tt}, \sigma_{\varphi\varphi})$ are the diagonal components of the bulk stress tensor in the membrane shell in the two principal directions.

Viscous contribution The cortex is a Maxwell viscoelastic material. It flows therefore as a fluid at long timescales compared to its viscoelastic relaxation time (5). This time is necessarily smaller than the turnover time of the layer since elastic stresses accumulated in the material are released during its renewal. The cell shape deformation occurs at timescales much larger than the typical turnover time of the cortex (5), and inertia is largely negligible at these lengthscales. We can therefore consider the cortex as a Stokes fluid, the constitutive equation of which reads (6)

$$\sigma_{ij} = 2\eta \, v_{ij} - p \, \delta_{ij}. \tag{7}$$

where $v_{ij} \equiv \frac{\partial_i v_j + \partial_j v_i}{2}$ is the symmetric strain-rate tensor, which is naturally diagonal for an axisymmetric membrane shell in our local Frenet frame $(\boldsymbol{t}, \boldsymbol{n}, \boldsymbol{e_\varphi})$

$$v_{ij} = \begin{pmatrix} v_{tt} & 0 & 0 \\ 0 & v_{nn} & 0 \\ 0 & 0 & v_{\varphi\varphi} \end{pmatrix}. \tag{8}$$

The normal component of the stress vanishes for a mechanical membrane shell: $\sigma_{nn} \approx 0$ (3), which allows us to determine the isotropic part $-p$ of the stress with the help of incompressibility: $p = -2\eta\,(v_{tt} + v_{\varphi\varphi})$

The viscous contributions to tangential and azimuthal membrane shell tensions reduce therefore to:

$$\tau_t^v = 2\eta\, e\,(2v_{tt} + v_{\varphi\varphi})\,, \tag{9a}$$

$$\tau_\varphi^v = 2\eta\, e\,(2v_{\varphi\varphi} + v_{tt})\,. \tag{9b}$$

Active contribution The active-gel theory predicts a contractile active stress contribution of the form $\sigma_{ij} = \zeta\Delta\mu\langle p_i p_j - \frac{1}{3}\delta_{ij}\rangle$ (41), where $\zeta > 0$ is a measure of the local motor contractile activity, $\Delta\mu$ is the chemical energy difference associated with the hydrolysis of an ATP molecule, p_i represents the local polarity and $\langle\,\rangle$ denotes an average over a typical mesoscopic lengthscale. For sake of simplicity we assume here that the filaments remain parallel to the membrane shell mid-surface and isotropically distributed in the plane of the cortex. The active contribution to cortical tension is therefore isotropic and reads simply

$$\tau_t^a = \tau_\varphi^a = \frac{e}{2}\,\zeta\Delta\mu. \tag{10}$$

Total tensions The cortical tensions are hence the sum of an isotropic active term (Eq. 10) and an anisotropic viscous term (Eqs. 9). Both are proportional to the local cortical thickness e:

$$\tau_t = \frac{e}{2}\,\zeta\Delta\mu + 2\eta\, e\,(2v_{tt} + v_{\varphi\varphi})\,, \tag{11a}$$

$$\tau_\varphi = \frac{e}{2}\,\zeta\Delta\mu + 2\eta\, e\,(2v_{\varphi\varphi} + v_{tt})\,. \tag{11b}$$

Turnover dynamics

The cortex is under permanent rapid turnover (5). Actin polymerization nucleators are generally localized in the vicinity of the plasma membrane whereas depolymerization acts in bulk. This leads respectively to a polymerization velocity v_p away from the plasma membrane and a bulk depolymerization rate k_d. The mass conservation equation reads

$$\frac{1}{Se}\frac{DSe}{Dt} = v_{tt} + v_{\varphi\varphi} + \frac{1}{e}\frac{De}{Dt} = \frac{v_p}{e} - k_d. \tag{12}$$

where time derivatives are material derivatives.

We define the stationary thickness e_0 by $\frac{DSe_0}{Dt} \equiv 0$ which leads to:

$$e_0 = \frac{v_p}{k_d}. \tag{13}$$

The turnover dynamics is therefore a process that tends to maintain a uniform cortical thickness $e \sim e_0$ with some typical relaxation time scale k_d^{-1}.

Local perturbation from the sphere

Starting from a spherical membrane shell as sketched in Fig. S3 A, of radius R_0 and thickness e_0 at mechanical equilibrium, i.e. verifying Laplace's law

$$\Delta P = \frac{\tau_t + \tau_\varphi}{R_0} = \frac{2\tau_t}{R_0} = \frac{\zeta_0\Delta\mu e_0}{R_0}. \tag{14}$$

We perturb the membrane shell in a small region of typical size $\frac{a}{R_0}$, at the pole $\theta = 0$ of the cell. We decrease slightly the local active tension, either through the myosin activity $\zeta = \zeta_0 - \delta\zeta$ or via the polymerization $v_p = k_d\, e_0 - \delta v_p$.

Linearization of equations around the sphere

We perturb the variables around the sphere and choose the angle $\theta \equiv \frac{s_0}{R_0}$ as the coordinate

$$\begin{aligned}
&\psi(\theta) = \theta + \delta\psi(\theta)\,, && R(\theta) = R_0 + \delta R(\theta)\,,\\
&e(\theta) = e_0 + \delta e(\theta)\,, && r(\theta) = r_0(\theta) + \delta r(\theta)\,,\\
&v_p(\theta) = e_0\, k_d + \delta v_p(\theta)\,, && \kappa_t(\theta) = \tfrac{1}{R_0} + \delta\kappa_t(\theta)\,,\\
&\zeta(\theta) = \zeta_0 + \delta\zeta(\theta)\,, && \kappa_\varphi(\theta) = \tfrac{1}{R_0} + \delta\kappa_\varphi(\theta)\,,\\
&P = P_{\rm int0} + \delta P_{\rm int}\,.
\end{aligned}$$

We rescale the variables as follows to make them dimensionless

$$\begin{aligned}
&\bar{R} = R/R_0\,, && \bar{t} = t\,\tfrac{\zeta_0\Delta\mu}{2\eta}\,,\\
&\bar{\kappa}_t = R_0\,\kappa_t\,, && \bar{v}_{\rm p} = \tfrac{v_{\rm p}}{e_0\,k_d}\,,\\
&\bar{\kappa}_\varphi = R_0\,\kappa_\varphi\,, && \bar{k}_{\rm d} = k_{\rm d}\,\tfrac{2\eta}{\zeta_0\Delta\mu}\,,\\
&\bar{e} = e/e_0\,, && \bar{u}_{\alpha\alpha} = u_{\alpha\alpha}\,\tfrac{2\eta}{\zeta_0\Delta\mu}\,,\\
&\bar{\zeta} = \zeta/\zeta_0\,, && \bar{P} = \tfrac{P}{\zeta_0\Delta\mu}\,\tfrac{R_0}{e_0}\,.
\end{aligned}$$

From force balance and turnover dynamics (Eqs. 1, 4 and 12) we get three coupled linearized and dimensionless equations describing the quasi-static mechanical equilibrium of the membrane shell. We omit the upper-bar from here on for sake of readability.

$$\delta P_{\rm int} = \delta e + \delta\zeta + 3\,(u_{tt} + u_{\varphi\varphi}) + \frac{1}{2}\,(\delta\kappa_t + \delta\kappa_\varphi)\,, \tag{15a}$$

$$0 = \partial_\theta\,\delta e + \partial_\theta\,\delta\zeta + 2\,[\partial_\theta\,(2u_{tt} + u_{\varphi\varphi}) + \cot\theta\,(v_{tt} - v_{\varphi\varphi})]\,, \tag{15b}$$

$$0 = k_{\rm d}\,[\delta e - \delta v_{\rm p}] + u_{tt} + u_{\varphi\varphi} + \frac{d\delta e}{dt}. \tag{15c}$$

The geometric variables are not independent from each others and one can easily show that

$$\delta\kappa_t = -\left\{\partial_\theta^2 + 1\right\}\,\delta R, \tag{16a}$$

$$\delta\kappa_\varphi = -\left\{\cot\theta\,\partial_\theta - 1\right\}\,\delta R. \tag{16b}$$

We can also express the strain rates as a function of the velocities (v_θ, v_R) along the directions $(\mathbf{e}_\theta, \mathbf{e}_R)$ at first order in perturbation:

$$v_{tt} = \partial_\theta v_\theta + v_R, \tag{17a}$$

$$v_{\varphi\varphi} = \cot\theta\, v_\theta + v_R. \tag{17b}$$

Local perturbation of activity or/and turnover in the bead region

We look at the response of the cell to the combined effect of a prescribed polymerization and myosin activity decrease in the region of the bead.

$$\delta v_p(\theta) = -\delta v_p^B\, e^{-\left(\frac{\theta}{\theta_B}\right)^2}, \tag{18a}$$

$$\delta\zeta(\theta) = -\delta\zeta_B\, e^{-\left(\frac{\theta}{\theta_B}\right)^2}. \tag{18b}$$

where $\theta_B \equiv \arcsin\left(\frac{a}{R_0}\right)$ with a the size of the perturbation region. $\delta v_p^B > 0$ and $\delta\zeta_B$ are the amplitude of, respectively, the polymerization and activity decrease in the cue region.

We seek for a stationary equilibrium solution of Eqs. 15, 16 and 17, which imposes $v_R \equiv \frac{1}{R}\frac{DR}{dt} = 0$ and $\frac{De}{Dt} = 0$. We therefore infer

$$\frac{1}{2}\left\{\partial_\theta^2 + \cot\theta\,\partial_\theta + 2\right\}\,\delta R = 3\left\{\partial_\theta + \cot\theta\right\}\,v_\theta + \delta e + \delta\zeta\,, \tag{19a}$$

$$4\left\{\partial_\theta^2 + \cot\theta\,\partial_\theta - \cot^2\theta - \frac{1}{2}\right\}\,v_\theta = -\partial_\theta\,\delta e - \partial_\theta\,\delta\zeta\,, \tag{19b}$$

$$-k_{\rm d}\,\left[\delta e - \delta v_{\rm p}\right] = \left\{\partial_\theta + \cot\theta\right\}\,v_\theta. \tag{19c}$$

We can check that we have three variables v_θ, δe and δR and three coupled differential equations. We therefore only need to precise the boundary conditions at $\theta = 0$ and $\theta = \pi$ to fully determine the solution of the problem subject to the external perturbations $\delta\zeta(\theta)$ and $\delta v_p(\theta)$:

$$v_\theta(0) = v_\theta(\pi) = 0, \tag{20a}$$

$$\partial_\theta R(0) = \partial_\theta R(\pi) = 0, \tag{20b}$$

$$\partial_\theta e(0) = \partial_\theta e(\pi) = 0. \tag{20c}$$

We decompose the variables in series of Legendre polynomials since these functions form is well-adapted to problems close to circular geometries:

$$v_\theta(\theta) = \sum_{n=1}^{+\infty} V^{(n)}\,\frac{\mathcal{I}_{n+1}(\cos\theta)}{\sin\theta}, \tag{21a}$$

$$\delta e(\theta) = \sum_{n=0}^{+\infty} E^{(n)}\,\mathcal{P}_n(\cos\theta), \tag{21b}$$

$$\delta R(\theta) = \sum_{n=0}^{+\infty} R^{(n)}\,\mathcal{P}_n(\cos\theta), \tag{21c}$$

$$\delta\zeta(\theta) = \sum_{n=0}^{+\infty} Z^{(n)}\,\mathcal{P}_n(\cos\theta), \tag{21d}$$

$$\delta P_{\rm int} = \sum_{n=0}^{+\infty} P_{\rm int}^{(n)}\,\mathcal{P}_n(\cos\theta) = P_{\rm int}^{(0)}. \tag{21e}$$

where $\mathcal{P}_n$ is the Legendre polynomial of order n and $\mathcal{I}_{n+1} \equiv \frac{\mathcal{P}_{n-1} - \mathcal{P}_{n+1}}{2n+1}$ is the Gegenbauer polynomial of order $n+1$.

We insert the previous decompositions into the stationary mechanical equilibrium Eqs. 19. By using classical properties of Legendre polynomials we get the following recursion relations between series coefficients: $\forall\, n \geq 1$

$$\frac{1}{2}\left[2 - n\,(n+1)\right]\,R^{(n)} = 3V^{(n)} + E^{(n)} + Z^{(n)}, \tag{22a}$$

$$2\left[1 - 2\,n\,(n+1)\right]\,V^{(n)} = n\,(n+1)\left[E^{(n)} + Z^{(n)}\right], \tag{22b}$$

$$V^{(n)} = -k_{\rm d}\,\left[E^{(n)} - V_p^{(n)}\right]. \tag{22c}$$

Mode $n = 0$ The mode $n = 0$ corresponds to an isotropic expansion of the cell, so $V^{(0)} = 0$. Because we consider that the cell volume does not vary we impose $R^{(0)} = 0$. Therefore only internal pressure has to increase to compensate the activity variation. Higher modes, on the contrary, conserve volume at first-order and do not contribute to pressure variation.

$$R^{(0)} = 0, \tag{23a}$$

$$V^{(0)} = 0, \tag{23b}$$

$$E^{(0)} = 0, \tag{23c}$$

$$P_{\text{int}}^{(0)} = Z^{(0)}. \tag{23d}$$

Mode $n = 1$ The mode $n = 1$ is treated separately since Eqs. 22a and 22b become degenerated which leaves $R^{(1)}$ undefined. This mode corresponds to a cell translation along the z axis and we impose here that the cell does not move along the z-axis according to experiments, so $R^{(1)} = 0$.

$$R^{(1)} = 0, \tag{24a}$$

$$V^{(1)} = \frac{k_d\, V_p^{(1)}}{1 - 3k_d}, \tag{24b}$$

$$E^{(1)} = \frac{3k_d\, V_p^{(1)}}{3k_d - 1}. \tag{24c}$$

Modes $n > 1$ For modes $n > 1$ the determinant of the system of Eqs. 22 is non-zero and we can solve it:

$$R^{(n)} = \frac{2\, k_{\text{d}} \left\{ V_p^{(n)} + Z^{(n)} \right\}}{2\, k_{\text{d}} \left[1 - 2n\,(n+1)\right] + n\,(n+1)}, \tag{25a}$$

$$V^{(n)} = \frac{k_{\text{d}}\, n\,(n+1) \left\{ V_p^{(n)} + Z^{(n)} \right\}}{2\, k_{\text{d}} \left[1 - 2n\,(n+1)\right] + n\,(n+1)}, \tag{25b}$$

$$E^{(n)} = \frac{2\, k_{\text{d}} \left[1 - 2n\,(n+1)\right]\, V_p^{(n)} - n\,(n+1)\, Z^{(n)}}{2\, k_{\text{d}} \left[1 - 2n\,(n+1)\right] + n\,(n+1)}. \tag{25c}$$

By calculating the coefficients $Z^{(n)}$ and $V^{(n)}$ from the expression of motor activity and polymerization perturbation (Eqs. 18a and 18b)

$$Z^{(n)} = \frac{2n+1}{2} \int_0^\pi d\theta\, \delta\zeta(\theta)\, \mathcal{P}_n(\theta) \sin\theta, \tag{26a}$$

$$V_p^{(n)} = \frac{2n+1}{2} \int_0^\pi d\theta\, \delta v_p(\theta)\, \mathcal{P}_n(\theta) \sin\theta. \tag{26b}$$

we can reconstruct numerically the functions $\delta v_\theta(\theta)$, $\delta e(\theta)$ and $\delta R(\theta)$, solutions of the problem by means of the formula (Eqs. 23, 24 and 25). The effects of the two perturbations, motor activity and polymerization, add up in Eq. 25, as expected for linearized equations.

Results of the model

Local decrease of active tension at the contact region with the bead triggers cell cortex and shape polarization

We impose successively in the bead region:

1: a decrease of motor activity ζ plotted in Fig. S3 B, while maintaining the polymerization v_p uniform along the cortex,

2: a decrease of the polymerization plotted in Fig. S3 C, while maintaining the motor activity ζ uniform along the cortex,

3: a simultaneous decrease of polymerization and myosin activity in the bead region as plotted in Fig. S3 D.

The three scenarios correspond to a decrease of the active tension in the region of the bead and lead to the same polarization process. The perturbation results in a longitudinal active flow that propagates along the cortex away from the bead toward the opposite pole. The flow velocity V, normalized by a typical active velocity $V_a \equiv R_0 \frac{\zeta_0 \Delta\mu}{2\eta}$, is zero at the two poles and has a maximum around the region where the activity perturbation vanishes (1:Fig. S3 B *Upper middle*, 2:Fig. S3 C *Lower middle* and 3:Fig. S3 D *Left*). This cortical flow tends to deplete actomyosin from the region of the bead and to accumulate it to the opposite pole. The competition of this flow with turnover dynamics, which tends to maintain a uniform thickness e_0 along the cortex, leads to a stationary distribution of cortical thickness (1:Fig. S3 B *Lower left*, 2:Fig. S3 C *Lower left* and 3: Fig. S3 D *Lower left*). The cortical flow leads to anisotropic viscous tensions along the cortex: $\tau_t^v(\theta) \neq \tau_\varphi^v(\theta)$ (1:Fig. S3 B *Lower middle*, 2:Fig. S3 C *Lower middle* and 3:Fig. S3 D *Lower middle*). We summarize the results in a plot of the cell shape, where we outlined the amplitude of the cortical flow via a color gradient (1:Fig. S3 B *Right*, 2:Fig. S3 C *Right* and 3:Fig. S3 D *Right* corresponding to Fig. 5 of the main text). The cell elongates along the polarization axis, leading to a pear-like shape which is in a good qualitative agreement with experimental observations of the polarized state of cells (Figs 1 A and 3 B; Fig. S2 B).

Cortical flows are necessary to account for non-spherical cell shapes

From a simple analysis of the equation of mechanical equilibrium (Eq. 4), we show that a purely isotropic cortical shell $\tau_t = \tau_\varphi$ leads to $\frac{\partial \tau_t}{\partial s} = 0$, i.e. to a constant surface tension along the cortex: $\tau_t = \tau_\varphi = \text{cte}$. From the equation of normal force balance (Eq. 1) we then deduce that the only solution for an isolated cell subject to isotropic tension and uniform pressure $\Delta P > 0$ is the spherical shape, which indeed minimizes optimally the surface for a given volume. The same arguments can account for the natural spherical shape of bubbles which is characterized by the seminal law of Laplace $\Delta P = \frac{2\gamma}{R_0}$ (where the coefficient 2 accounts for the two equal and uniform cortical tensions γ).

Since the active tension is isotropic by definition (see Eqs. 10), it also leads to a spherical cell shape, which is indeed the characteric mean shape adopted by isolated cells in suspension (Fig. 3 A; Fig. S2 A). To account mechanically for the non-spherical shapes of polarized cells (Figs. 1 A and 3 B; Fig. S2 B), the anisotropic contributions to the cortical tensions have to be invoked. They only emerge from a sustained cortical flow, which is necessarily anisotropic on a closed surface. This simple mechanical analysis predicts

therefore that non-spherical stationary shapes of the polarized cells are a strong evidence of a persistent and longitudinal cortical flow along their surface.

Further analysis of the plots of tensions within the cortical shell (Fig. S3 B-D) reveal common mechanical properties:

- The viscous tension along the azimuthal direction $\boldsymbol{e_\varphi}$ is systematically higher than the viscous tension along the tangential direction $\boldsymbol{t}$: $\tau^v_\varphi \geq \tau^v_t$. The cell is subject to higher tension along its azimuthal direction and elongates therefore along the transverse axis $\boldsymbol{e_z}$.
- The viscous tensions are equal at the poles: $\tau^v_t(\theta = 0) = \tau^v_\varphi(\theta = \pi) \equiv \tau^v$ making cortical tension locally isotropic. The two poles extrema, that we denote 1 for $\theta = 0$ and 2 for $\theta = \pi$, are therefore the only physical points where the cell is purely spherical and where the original law of Laplace applies: $\Delta P = \frac{2\left(\tau^a_{1,2}+\tau^v_{1,2}\right)}{R_{1,2}}$. Since the active contribution dominates largely over the viscous contribution in the cortical tension $\tau^a + \tau^v \approx \tau^a$ (note the multiplying factor 10 for viscous tensions in the plots), we can make a rough mechanical analysis of the curvature radius difference between these two points in experiments (Fig. 3 B *Trapped at 30'*): the actomyosin has been depleted from region 1 (bead $\theta = 0$) and enriched in region 2 (opposite pole $\theta = \pi$), which leads to a stronger active, and therefore cortical tension in the region 2. Since the pressure is uniform within the cell at equilibrium, the law of Laplace reads $\frac{R_2}{R_1} \approx \frac{\tau^a_2}{\tau^a_1} > 1$. The radius of curvature in the region of the bead is indeed clearly lower than the one at the opposite pole (Fig. 3 B *Trapped at 30'*). Because of the adhesion surface of the bead, one can remark nevertheless that the cell can not be perfectly spherical experimentally at this point.

Supporting References

1. Kruse, K., J. F. Joanny, F. Julicher, J. Prost, and K. Sekimoto. 2005. Generic theory of active polar gels: a paradigm for cytoskeletal dynamics. Eur Phys J E Soft Matter 16:5-16.
2. Turlier, H., B. Audoly, J. Prost, and J. F. Joanny. 2014. Furrow constriction in animal cell cytokinesis. Biophys J 106:114-123.
3. Green, A. E., and W. Zerna. 2002. Theoritical Elasticity, (eds) pp. 286-289. Dover Publications.
4. Berk, D., and E. Evans. 1991. Detachment of agglutinin-bonded red blood cells. III. Mechanical analysis for large contact areas. Biophys J 59:861-872.
5. Salbreux, G., G. Charras, and E. Paluch. 2012. Actin cortex mechanics and cellular morphogenesis. Trends Cell Biol 22:536-545.
6. Hapel, J., and H. Brenner. 1983. Low Reynolds Number Hydrodynamics. Kluwer Academic Publishers.